The Detection of Structural Defects in GaAs by Electrochemical Etching

M. M. Faktor and J. L. Stevenson

Post Office Research Centre, Martlesham Heath, Ipswich, Suffolk, IP5 7RE England

ABSTRACT

Two methods of anodically etching n-GaAs have been investigated. Subsequently they have been used to detect crystallographic defects present in bulk-grown, single crystal material. The first method provides topographical featuring of the semiconductor anode. The selective discrimination of defects achieved via this controlled electrochemical technique is superior to that obtainable from standard chemical etchants. The second dissolution regime, in which an interfacial oxide layer is continuously present, permits smooth, featureless removal of material. Thus a simple two-stage anodization procedure has allowed the damage characteristic of the Beilby layer to be probed. Thereafter, a total, smooth removal of this damaged surface layer permits identification of bulk crystallographic defects—dislocation structures well known in GaAs require the dissolution of only 0.5 μm. Analysis of the semiconductor electrode condition in the electrolytes used for etching has yielded model results. Such analyses have enabled the relationship between the electrical properties of the defected GaAs and the individual topography of the defects as etched to be explored.

The electrochemical characteristics of gallium arsenide and other III-V semiconductors have recently attracted increasing interest. As well as providing a route for an automated electrical assessment of both epitaxial and substrate quality material (1, 2), anodic oxide films have been intensively studied (3, 4), mostly in connection with MOS device applications utilizing GaAs.

The studies reported here have some relation to both of these topics, but are differently aimed overall. It has become increasingly clear in the production of liquid-phase epitaxial GaAs and $Ga_xAl_{1-x}As$ for optoelectronic devices that routine evaluation of the material should center on the crystallographic defect content of the epilayers (5). Some defects act as nonradiative, enhanced recombination centers, which reduce the efficiency of photoabsorptive devices (solar cells) and which degrade and may terminate the efficiency of photoemissive units (lasers) (6). Chemical etching would appear to provide the technically easiest means of defect identification once the etchant has been calibrated (7). However, the current state of the art is inadequate for the purpose indicated. Optical resolution of etch pits in single $Ga_xAl_{1-x}As$ layers has recently been reported by Komiya *et al.* (8) as possible only after the dissolution of 4 μm in a H_2O_2/HF solution. For GaAs/$Ga_xAl_{1-x}As$ double heterostructure material, where all five epilayers together occupy about this very thickness (9), a ten-fold improvement in the resolution achieved per unit depth probed would be the minimum desired. Although defect detection in heterostructures has been displayed (5) via the use of the AB etchant (10) in a modified form, an extra thickness of epitaxial growth was necessitated in order to accommodate the lack of etch discrimination.

Both Ambridge *et al.* (1) and Niehaus and Schwartz (3) were able to report in the work already cited that electrolytic etching of GaAs produced features at the electrode surface. These were presumed related to the defects in the sample. Kuhn-Kuhnenfeld (11) used a chemical etchant of standard composition for GaAs under conditions where the photovoltaic properties of the semiconductor provided effective electrolytic control. Although the procedure was not subjected to a critical calibration, various features became well resolved after 2 μm of etching. Several appeared "dislocation like." Later Saitoh *et al.* (12) used the same scheme of photoassistance together with the AB etch composition and were able to gain a good delineation of defects with the removal of less than 1 μm of material.

Key words: gallium arsenide, electroetching, oxide films, dislocations, striations.

We report here on the development of two complementary techniques of anodic dissolution of n-GaAs; one to yield a topographically featured surface, and the second to allow continuous, smooth etching. The electrode polarization studies which preceded the design of each technique are detailed in an Appendix. Correlation of the morphological detail displayed via the first etching mode has been carried out with the use of double crystal x-ray reflection topographs. The selective resolution of defects such as dislocations by our electrochemical technique is shown to be superior to that obtained from other currently advocated etching techniques (7). Minimal dissolution is required (0.5 μm or less) close to the target set.

In this instance, our attention is given to bulk-grown n-GaAs alone. Therefore we are describing the trial of these methods on substrate quality material. However, as a specific example of the resolution capability and to illustrate how the procedures can be used to profile the defect content of a GaAs slice in depth with high accuracy the differentiation of surface damage and bulk defects close to the surface of a substrate are described.

Experimental

Much of the apparatus used in this work has been described previously by Ambridge *et al.* (1, 2). A major difference here, however, concerned the cell construction, where an all-glass unit was designed. This was basically a small spectrophotometer cell with a PVC sample mounting ring (2) mounted directly onto one face which had been predrilled as appropriate. There were, as before, inlet/outlet ports for electrolyte flow and limbs for the insertion of a saturated calomel reference electrode and a carbon cathode. A platinum wire electrode for capacitance measurements was inserted directly through the side of the PVC ring. Both the sealing of the GaAs sample onto the ring and the provision of electrical contact to it were achieved via sprung probes of tin-coated gold wire (2).

By mounting the cell directly onto a microscope stage plate and using an inverted metallurgical microscope, observation of the whole exposed GaAs electrode surface (~7 mm^2) was possible at a magnifica-

tion of 30× (at the eyepiece). Examination of fine topographical details developed during anodization such as etch pits, areas of nondissolution, and surface film nucleation sites was very straightforward. Illumination of the electrode was direct via the microscope optics and since all of the polarization behavior reported here involves illumination, a continuous visual observation of the electrode was possible. The optical source was a 250W high pressure mercury arc lamp set to provide Koehler irradiance of the sample.

Measurement of electrode potential was obtained through a high impedance digital voltmeter (Solartron LM 1604). An autobalance capacitance bridge (Wayne Kerr B641), operating at 1.592 kHz, was used for measurement of interfacial capacity. Polarization of the illuminated electrode was attained by use of the potentiostat designed by Bremner *et al.* (13). Cell current was monitored using an electrometer (Keithley Model 602) with its output facility linked to a digital integrator (Time Electronics TS100A). Two electrolytes new to GaAs electrochemistry were used throughout this work. They were: as stock solutions, 0.5M Tiron (1,2 dihydroxybenzene-3,5 disulfonic acid disodium salt) which had a pH = 3.45; and 0.3M sodium dihydrogen orthophosphate pH = 4.32. The GaAs used had been boat grown and cut into slices in a {100} orientation (Mining and Chemical Products Limited and Monsanto Chemicals Limited). All were silicon doped.

Electrochemical Characteristics and Technique

Electrode capacitance.—Reproducible Mott-Schottky characteristics were obtained from unilluminated n-GaAs ($N_d = 2.0 \times 10^{17}$ cm^{-3}) electrodes (14) using both of the electrolytes chosen for use here. The flatband and open-circuit potentials are plotted in Fig. 1 together with previously published data.

Electrode polarization.—Illumination of the same electrode samples yielded sizable photopotentials (~ −450 mV) and, in the usual manner, allowed stable anodic polarization (reverse-biasing of the Mott-Schottky barrier) curves to be obtained (Fig. 2). Current/voltage behavior was also examined using various solutions formed by mixing the two basic electrolytes.

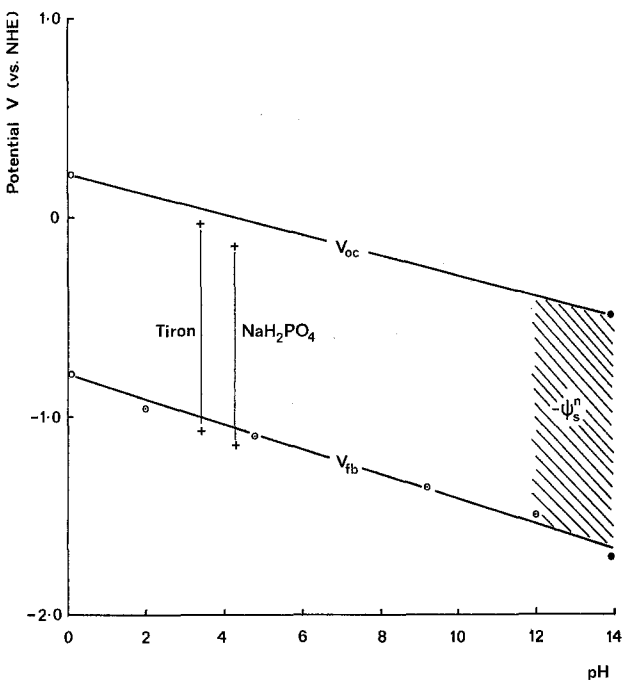

Fig. 1. Collation of data concerning the variation in band bending at the unilluminated n-GaAs electrode with electrolyte pH. Values for the flatband potential (V_{FB}) and the open-circuit (rest) potential (V_{oc}) are taken as follows: ○ Benard and Handler (29); ⊙ LaFlere *et al.* (41); ● Ambridge and Faktor (14).

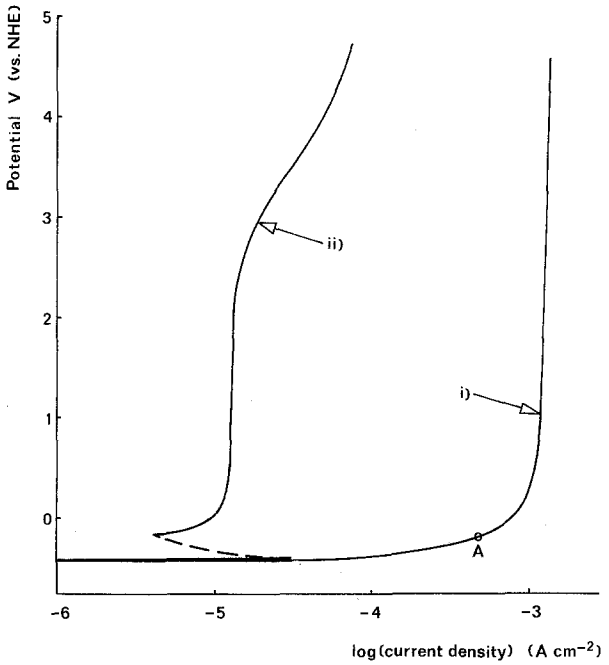

Fig. 2. Current-voltage behavior of an illuminated n-GaAs electrode (same sample as Fig. 1) in: i. 0.5M Tiron; and ii. 0.3M NaH_2PO_4. The point A marks the experimental condition for step 2, Fig. 5.

For example, it was found that only small proportions of Tiron (10% v/v) were required in the electrolyte to yield current characteristics identical to Fig. 2i. In this case, the reverse-bias breakdown behavior of a lower doped n-GaAs electrode was examined—again with illumination—and found to be as plotted in Fig. 3.

Electrode morphology.—Since all of the curves such as shown in Fig. 2 and 3 were gained with an experimental arrangement which allowed direct visual inspection of the electrode, the surface morphology developed was very easily relatable to particular polarization conditions. The photographs in Fig. 4 are representative of etching under steady-state conditions at the points marked A in Fig. 2i and B in Fig. 3.

The result of the single etching experiment shown as Fig. 4i bears no similarity to morphologies found either by Kuhn-Kuhnenfeld (11) or Saitoh *et al.* (12)

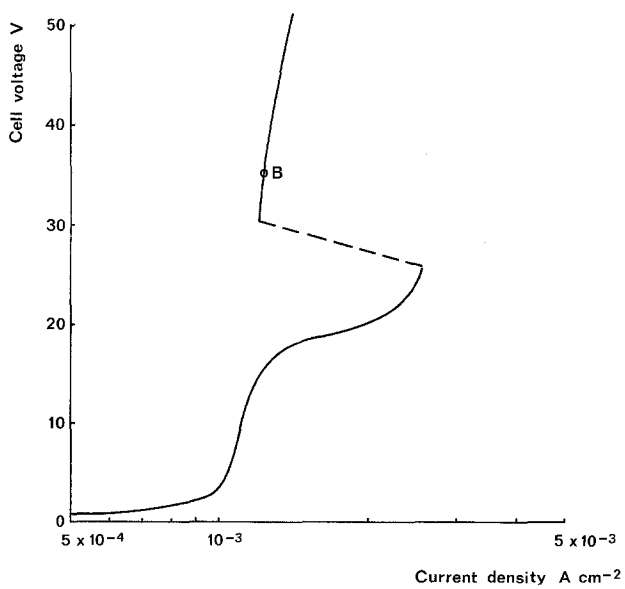

Fig. 3. Extended current-voltage plot for an illuminated n-GaAs electrode (2.6 × 10^{16} donors per cm^3) in a mixed electrolyte (10% 0.5M Tiron/90% 0.3M NaH_2PO_4). The point B marks the experimental condition for step 1, Fig. 5.

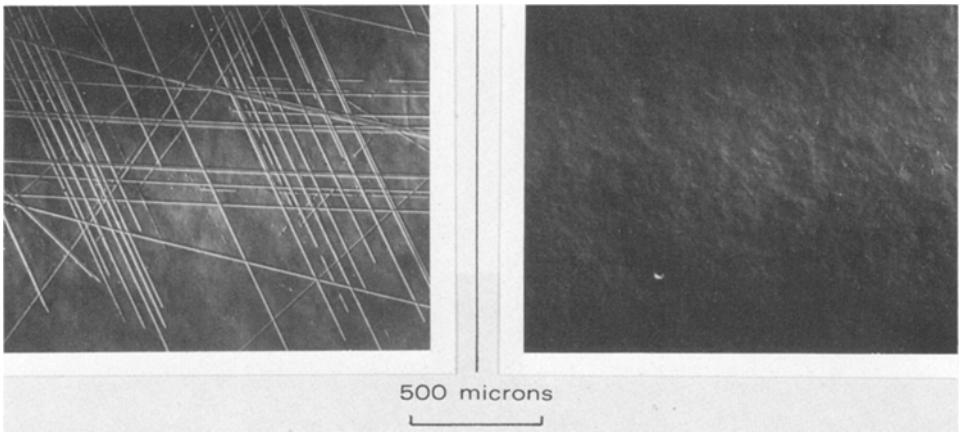

Fig. 4. Photomicrographs (Nomarski interferometry) showing surface morphologies developed after electrochemical etching of two separate samples: i. at point A in Fig. 2i, 0.2 μm removed; and ii. at point B in Fig. 3, 5.2 μm removed.

in those studies of the photoassisted chemical dissolution of n-GaAs which we judge to be closest to our fully controlled electrochemical conditions. In our case, the sample used had been mechanochemically polished using a standard bromine/methanol routine immediately prior to anodization. It appeared, therefore, that the low overpotential etching in Tiron solution had revealed features representing imperfections introduced during the sample preparation. This supposition was confirmed by subjecting similarly finished slices to a sequential etching experiment as indicated in Fig. 5. Step 1 was accomplished by use of the defect-independent etching conditions (point B in Fig. 3) leaving a surface typically as that shown in Fig. 4ii. Then after a simple replacement of electrolyte, step 2 was initiated and the surface topography monitored through its duration using the microscope. Both d_1 and d_2—the successive etch depths— were easily calculable via the integrated current density (for details, see the Appendix). As an example, the two etched surfaces pictured in Fig. 6i and 6iv were obtained with material removals of $d_1 = 2.0$ μm and $d_2 = 0.57$ μm. The minimum value of d_1 found necessary in order to avoid the appearance of etch features caused by polishing damage was 0.5 μm for the mechanochemically polished slices.

Crystallographic Defect Studies

We shall begin here with comments concerning the polishing damage encountered during the single etch experiments. Clearly no information concerning the bulk defect structure of n-GaAs substrate wafers can be obtained definitively without the removal of the damaged surface layer.

In fact, the appearance of prepolished surfaces after a single step 2 etch changed quite sharply with prior alteration of the polishing rate (this made principally by varying the bromine content of the polishing solution). Where low rates had been used, the surface took on a continuously disturbed form, with all of the linear features as per Fig. 4i in close coalescence. Thus a form of Beilby layer (15) was present. Its characteristic

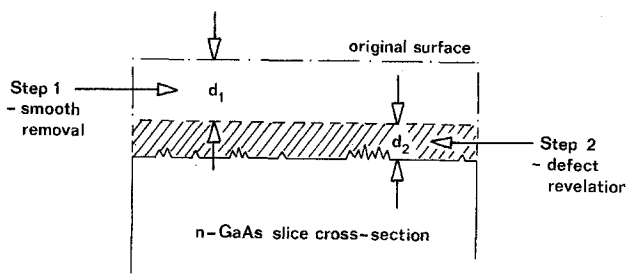

Fig. 5. Schematic representation of the sequential electrochemical etching experiment. The cross-hatched region marks the "layer" probed for defect content.

depth was, however, no different from that exhibited by the discretely scratched surface. The damage itself might arise from particles of abrasive material or even GaAs which have remained attached to the slice after any mechanical treatment, or, more probably, have become trapped on the polishing pad at any time since its manufacture. We note that in spite of warnings to the contrary (7), mechanochemically prepared GaAs slices are still taken to be damage free (16). Our ability here to reveal minor work damage, such as that caused by mechanochemical polishing, and to profile its region of confinement near the surface at submicron levels, illustrates nicely the fine resolution of defective material attainable with the electrochemical etching methods.

With regard to the crystallographic imperfections of the bulk, the etched slice photographed in Fig. 6i is only one of a number which have been subjected to a cross correlation with structural defect analysis by x-ray methods. Double crystal x-ray reflection topography was chosen—it has the advantage of probing a near surface layer alone (17, 18). More generally the two techniques used over-all then have independent origins, particularly so, as we shall show later, with the etching performed electrolytically. The x-ray topography was used first to map as fully as possible the defect content of the sample. Since not all possible dislocation Burgers' vectors will yield contrast at a single reflection, only a superposition of two x-ray topographs will provide a complete map of the dislocation distribution. Figures 6ii and 6iii are micrographs of the photographic plates on which the two x-ray exposures covering the same area were recorded, but the superposition is made difficult because the topographs are unavoidably distorted geometrically with their foreshortened axes perpendicular. Attempts at reaching a graphical correspondence between all three topographs, that is including the detail available after the sequential etching of the same sample area (Fig. 6i), are further hindered by a significant disparity in the depth resolution of the techniques. The morphology of Fig. 6i resulted from a dissolution in the topographical etching mode (d_2) of 0.57 μm, while the surface layer thickness imaged by the x-ray technique was ~18 μm (17, 18). Hence there is involved here a sampling discrepancy factor of more than thirty.

In view of these problems, the over-all correlation is judged fairly satisfactory. Note first that the pronounced linear feature present at the left-hand edge of all three topographs is the result of a deliberate scratch mark made as a geographical reference point. Thereafter, particular correspondences can be seen between the linear array of features extending along the line of the arrow marked A in Fig. 6i and 6ii, and also between a group of features at B in both Fig. 6i and 6iii. The line of detail labeled A in Fig. 6ii contains several linear images (one is arrowed at a) which do not appear in the complementary x-ray topograph. Analysis

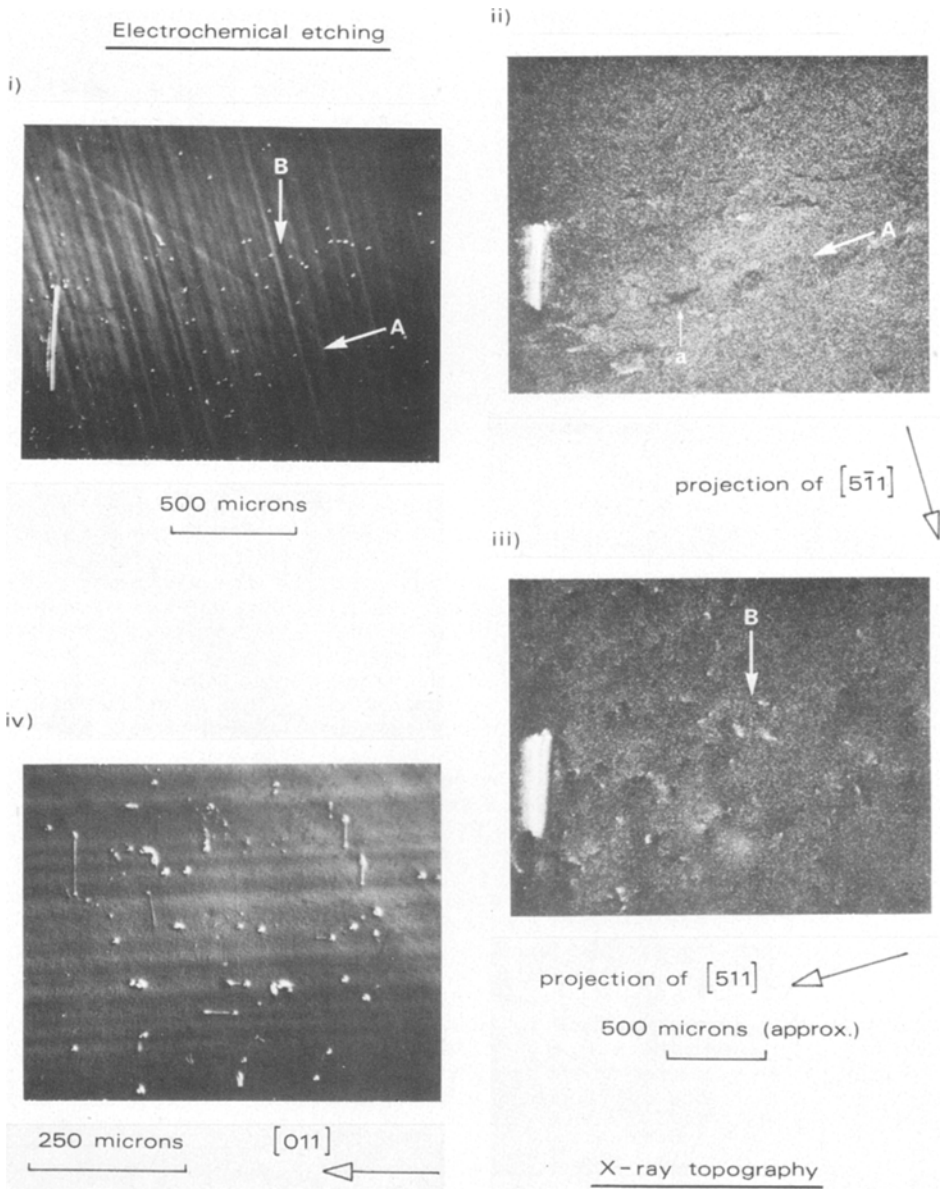

Fig. 6. Results of the etching calibration. i. Sample surface-morphology after electrochemical etching as indicated in Fig. 5, with d_2 0.57 μm; ii. and iii. double crystal x-ray reflection topographs recorded for the sample prior to etching, using the 5$\bar{1}$1 and 511 reflections from GaAs, respectively; and iv. features resulting from sequential electrochemical etching at an adjacent area to that shown as i. (n-GaAs sample, Si-doped, 8.6 $\times$ 10^{17} donors per cm^{-3}).

of the diffraction conditions show this to be a dislocation with a high (probably complete) edge component. Clearly it lies in a [011] direction. The absence of a comparable linear feature from the etched surface is probably attributable to the difference in depths probed, as described already. On a neighboring area of the same sample (which was not clearly imaged by the x-ray method due to slice curvature) the electrochemical etching did produce linear features arrayed along both the [011] and the [0$\bar{1}$1] directions (see Fig. 6iv, which has an increase in magnification and a sample rotation relative to Fig. 6i). Thus an ability to reveal both dislocation outcrops (for dislocations inclined to the surface plane) and dislocation lines (lying in the surface plane) is indicated. In this connection, note that the linear features present in Fig. 6iv are all terminated by a roundel, similar to those which, individually, represent dislocation outcrops. This indicates a segmentation of the dislocation into, presumably, the <110> directions and therefore at these points it either enters the bulk or was originally attached to the slice surface. Electron microscopy of bulk-grown GaAs has indicated previously that this dislocation type is often dominant (19).

The type and scale of defect discrimination demonstrated here is simply not attainable with many of the chemical etchants reported in the literature as suitable for defect analysis in GaAs (7), though the best characterized of these, the AB etch (10), may, under conditions of dilution (5, 20) and together with photoassistance (12), yield a comparable detection.

Some significant information concerning the mechanism by which defects are revealed in the step 2 electrolytic etching case can be gained by consideration of the data contained in Fig. 1 and 2i. (Note that an account of the characteristics contained in Fig. 1-3, together with their relation to previous work on the electrochemistry of GaAs, is given in the Appendix.) First, by using the surface barrier potential (ψ_s^n) shown for Tiron in Fig. 1, a band diagram for the appropriate semiconductor/electrolyte contact (at open-circuit, and unilluminated) can be constructed. This is shown as Fig. 7i. With subsequent illumination, the electron hole pairs photogenerated within the electrode produce a decrease in the barrier height while any anodic overpotential applied thereafter acts in the reverse-bias sense, assisting the diffusion of holes toward the interface. Under these circumstances, the photocurrent shown as Fig. 2i is produced. The diagram ii in Fig. 7 is a schematic representation of the electrode condition at point A on the polarization curve 2i where the anodic overpotential is +250 mV. If applied potentials in excess of 250 mV are used, a photocurrent saturation is attained and the electrode subjected to normal reverse-bias conditions, the depletion width increasing with voltage. Finally, on any further increase in potential, breakdown conditions will be approached.

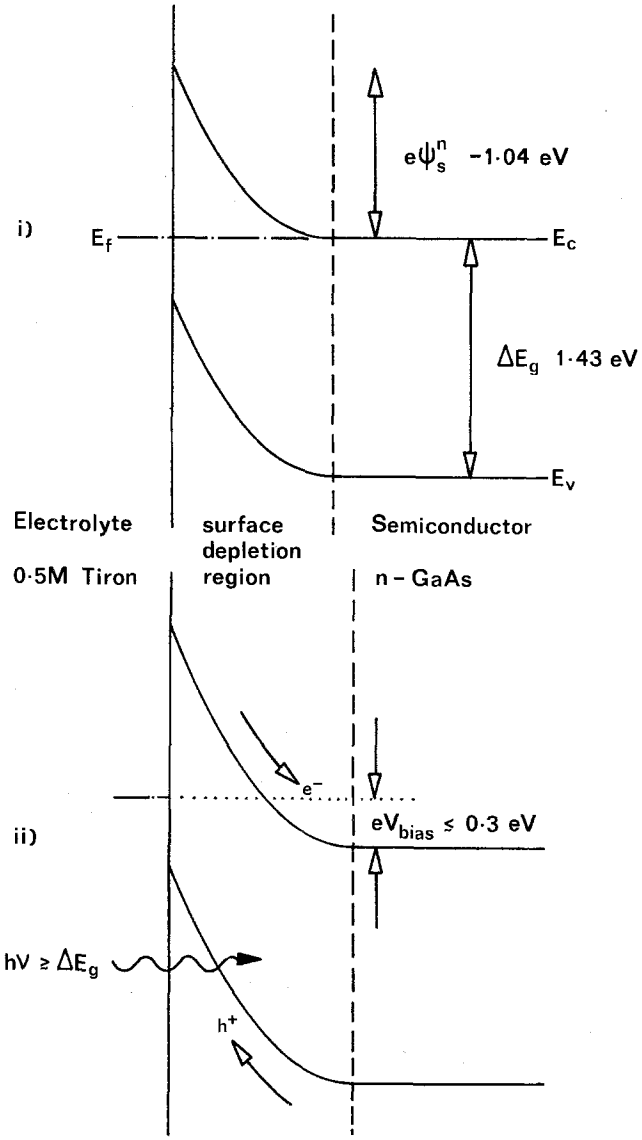

Fig. 7. Band diagrams representing: i. quantitatively, the n-GaAs electrode (unilluminated, and at the open-circuit condition) in contact with 0.5M Tiron electrolyte; and ii. schematically, the n-GaAs/0.5M Tiron half-cell under conditions represented by point A in Fig. 2i.

Any interband state acting as an electron-hole recombination center within the depletion width marked in Fig. 7ii will then introduce two localized perturbations to the over-all polarization behavior near the rest condition. First, there is a reduction in the open-circuit photopotential, and second, a stifling of the hole current which supplies the anodic dissolution reaction. Clearly the operation of the latter will produce points of low etching rate at the sites where nonradiative recombination processes are facile. It has long been well-known that dislocations can act as efficient nonradiative centers in most of the III-V compound semiconductors (21).

We have found that all of the discrete features etched on samples such as shown in Fig. 6i (where all of the defects are supposed characteristic of the bulk material) and Fig. 4i (where the defects arise from polishing operations) are indeed elevated in profile. This was ascertained by use of a Talysurf instrument on some heavily etched samples. The surface features produced on n-GaAs samples in both of the photoassisted chemical etching studies already referred to (11, 12) exhibited a similar cross-sectional geometry. Although Kuhn-Kuhnenfeld (11) recorded negative photopotentials—as happened here—and attempted an explanation of the etching action via his data, no ascription of a mechanism for defect delineation can be realistically made on the basis of such singular observations. This is because the overpotential available for the dissolution remains largely chemical in origin. Only by the addition of a full electrochemical control, as that obtained by our fixing of the electrode potential of the semiconductor sample, can the over-all mechanism depicted semiquantitatively in Fig. 7ii be justifiably proposed.

This contention is open to experimental test. Although at low overpotentials the localized recombination processes are responsible for impeding the dissolution, an increase in applied bias should lead to a reduction in defect resolution. This follows because the increased field strength imposed in the depletion region during the traversal of the photosaturation is responsible for a decrease in the probability of minority carrier trapping at the imperfection (22). There is an intrinsic mechanism involved (that is a field effect on the capture cross section of the trap) and probably also a contribution resulting from the increased energy imparted to the carrier (23). Thus the experiment consists of comparing the resolution of defects at different anodic potentials. The photomicrographs of Fig. 8 display the results obtained from such a study.

Two separate Si-doped samples were involved, labeled D and S, and clearly have very different defect morphologies. Each was examined at three adjacent areas. The micrographs Di and Si show the surface morphology obtained after "standard" sequential electrochemical etching, as per Fig. 5, with a step 2 overpotential of ≤ 300 mV and with $d_2 = 0.57$ μm and 0.40 μm, respectively. There is a significant discrepancy between the resolution attained for Di and that yielded by the sample shown in Fig. 6i and 6iv, even though the etching conditions were the same in each case. Their dissimilar behavior might be taken to indicate that a different degree or type of dislocation decoration was specific to each. The wafers had almost identical carrier concentrations, but originated from different manufacturers. This marked discrepancy in etch behavior was observed consistently through a whole range of samples obtained from these two suppliers. The topography shown by the sample S has, in the equivalent case(Si) two basic elements. The striations present in the left-hand portion of the micrograph were originally supposed to derive from a known facet effect often incurred during the bulk solidification of GaAs (24). Clearly some extensive microfaceting would be required to produce the features as observed. However, the same defected area gave a strongly imaged, banded contrast on an x-ray topograph. This is probably inconsistent with simple variations in dopant concentration alone (7). The common severity with which these features were resolved by both techniques leads us to suspect that they have a basic crystallographic origin, possibly linked to lamellar twinning (7). (Note that there are also striations present in Fig. 6i, but they are very much weaker than those of Si. Also the accompanying x-ray topographs there (6ii and 6iii) have no image matching the striae. Our conclusion is that these etch features do correlate with simple variations in dopant concentration, and hence carrier mobility, and that the periodic distribution arose there from thermal cycling occurring during solidification.) Also present for Si, and covering the whole area of the micrograph, is an array of small nodular features at a density of $\sim 2 \times 10^6$ cm^{-2}. Their origin is as yet uncertain. However, considering the carrier concentration of the sample ($N_d = 2.4 \times 10^{18}$ cm^{-3}), dopant precipitation would appear to be a strong possibility. Some attempts were made to check the comparative behavior of this wafer on use of the AB chemical etchant (10), both in a standard form and also with dilution and photoassistance together (12). Only in the latter case was a clear resolution of the same nodular topography attained. The concentrated etchant produced only a marginal featuring of the

surface, certainly not as clear a morphology as that observed for GaAs doped with Se and Te at the same concentration levels (25). For these materials, Stirland (25) has observed good correlation between etch pit features (at localized densities of between 10^6 and 10^8 cm^{-2}) and small defects allied to dopant precipitates. The evidence for the presence of similar imperfections in silicon-doped material is certainly much less clear and our result can only be advanced as an additional preliminary indication of similar precipitation effects.

The changes in the etch morphologies developed at different electrode potentials are shown in sections ii and iii of Fig. 8. The central pair of micrographs (Dii and Sii) illustrate the results gained after using an overpotential of 1.25V. (This is sufficient to double the possible voltage drop across the depletion region and therefore to increase the field strength relative to that of the first etching experiment by a factor of $\sqrt{2}$.) Interestingly, the resolution of each defect type is affected differently. The striated features (in Sii), the origin of which we have been unable to identify with complete confidence, remain as well resolved as in the initial case Si. In Dii, only those dislocations resolved most severely in the first instance have now produced a local perturbation of the anodic current, while the distinctive nodular features present in Si are no longer revealed at all in the second case. The material removal was held constant for each sample ($d_2 = 0.57$ and 0.40 μm were the average removals for D and S, respectively). At this stage we can conclude that the qualitative model dealing with the selective resolution of imperfections has been amply verified by the experi-

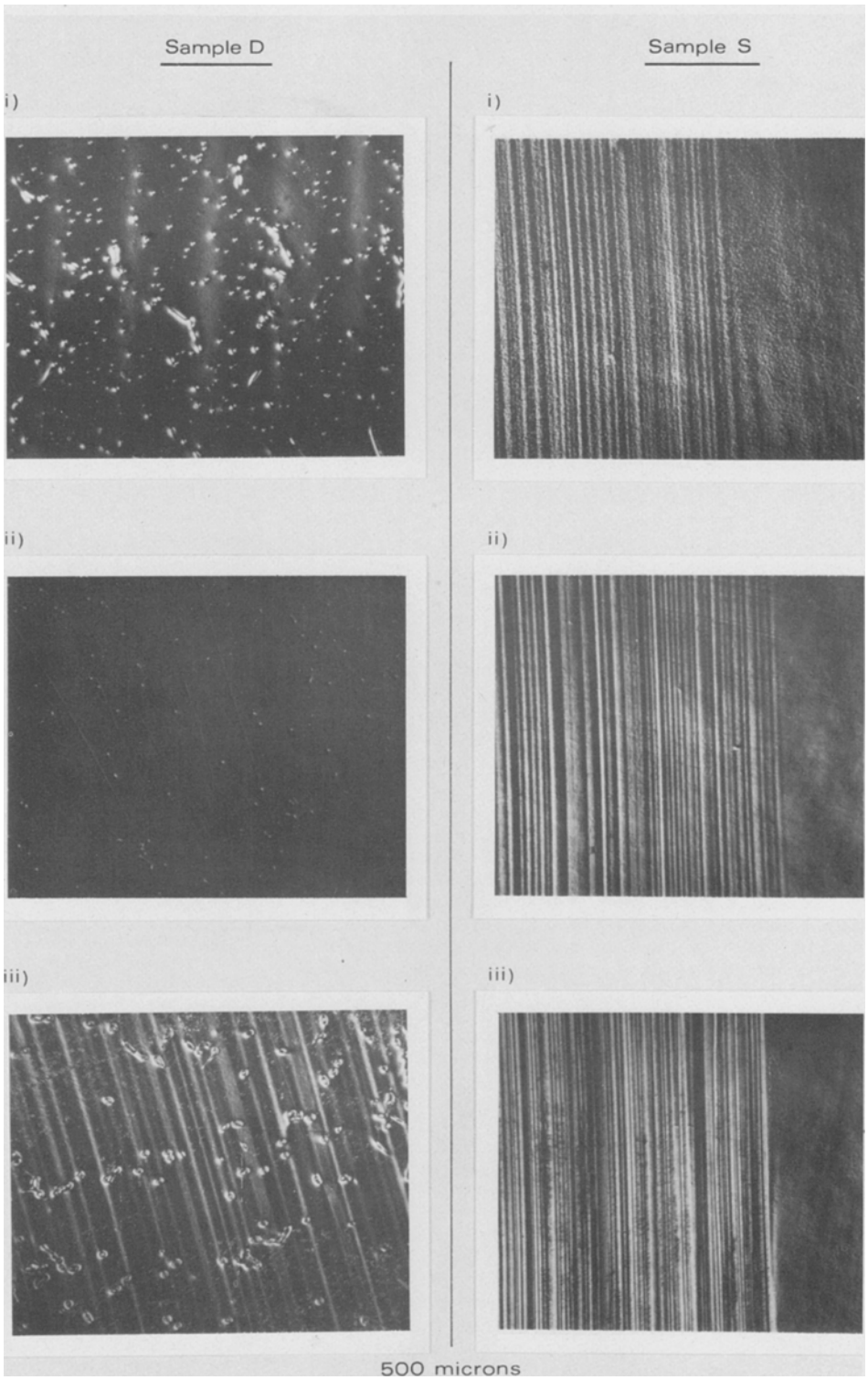

Fig. 8. Nomarski interference micrographs showing the etch morphologies developed during the defect revelation procedure at different anodic electrode potentials; i. overpotential ~250 mV; ii. overpotential 1.25V; iii. overpotential ≧ 1.75V. (n-GaAs samples: D, Si-doped, 7.8 × 10^{17} donors per cm^3; S, Si-doped, 2.4 × 10^{18} donors per cm^3).

mental results. Additionally, there appears to be available some semiquantitative information concerning the minority carrier lifetime at different defect centers.

In connection with this last statement, the results gained at current densities exceeding the photosaturation are of interest (Diii and Siii). The defects which were acting primarily as recombination centers in the low overpotential etching, should, under the necessarily higher overpotential conditions now required, participate as localized breakdown sites. The use of this etching regime is known from previous experiments to result in a discretely pitted surface (26, 27). Thus an inversion of the etch morphology is possible on traversing the whole anodic potential range. This is shown separately here in Fig. 9 by the comparative display of Talysurf traces for the two sample areas photographed as Di and Diii in Fig. 8. Because the electrochemical etching was confined to a well-defined circular area, the boundary etch step could be used for calibration of the vertical axis. These steps are positioned in line on the left-hand side of Fig. 9. The etch profile is then clearly resolved in both cases, consisting of elevated (ridged) features for Di and depressed (pitted) features for Diii. The edge step was also used to calibrate optical microinterferometers of the standard Michelson type and also a Nomarski differential interference contrast objective and use of these techniques confirmed that an inversion of etch topography was indeed gained on increasing the anodic potential. Finally, sample S was also subjected to etching at current densities > 1.5 mA cm^{-2}. In this case, (Siii), the dissolution is largely confined to the heavily striated material and the imperfections responsible for the nodular features in Si do not contribute individually to the reverse-bias breakdown of the sample area probed. The generation/recombination characteristics of each type of defect are clearly quite different.

Summary and Discussion

Our aim in this work was to procure a technically simple method for the resolution of crystallographic defects in GaAs, preferably with a resolution such that reproducible results could be gained with the removal of ≤ 0.5 μm of material. Of necessity, two previously untried methods of anodic dissolution have been investigated. The technique thus developed consists of:

(*i*) A defect-insensitive etch (step 1 in Fig. 5) which can be used for the removal of damaged material from as-polished surfaces, or to accurately section the slice to any predetermined depth. The anodic dissolution here is carried out continuously with an oxide film present at the interface to preserve the initial topography.

(*ii*) A defect-revealing etch for n-GaAs which has a high sensitivity related directly to the electronic characteristics of the imperfection (step 2 in Fig. 5).

Used in sequence, these two dissolution regimes allow: (*i*) the depth characteristic of polishing damage to be gauged quantitatively for any method of slice preparation; and (*ii*) the defect content of the bulk material (n-GaAs substrate) to be determined with a resolution not attainable with any of the standard chemical etchants used previously for GaAs.

One distinctive element of the technique described here has cardinal importance. The adoption of fully electrochemical etching conditions, in which chemical reaction between the etchant and semiconductor has been deliberately excluded, leaves the dissolution totally dominated by the optoelectronic properties of the sample. That is, etching only occurs at locations on the surface where the anodic current is either uninhibited or, alternatively, enhanced. Therefore the correlation of morphological features produced against defects identified by an independent crystallographic technique (as per Fig. 6) comprises a relation between the structural origin of the imperfection and its electronic consequence. Thus our experimental method corresponds quite closely to those adopted for detailed studies of structural defects and their nonradiative recombination characteristics in n-GaP (23, 28), except that in this case the etching and the optoelectronic probe are done neatly in combination.

Furthermore, the manner in which the semiconductor properties of GaAs dominate its electrode behavior indicates an easy extension of the method into analyses of epitaxial GaAs and probably also other III-V compounds. Working, for example, with the epitaxial structure of most interest at this time [the five-layer GaAs/$Ga_xAl_{1-x}As$ sequence grown for injection laser fabrication (9)], we have been able to probe the n-GaAs buffer material and its homoepitaxial interface with the substrate, and also, separately, the succeeding n-$Ga_{0.65}Al_{0.35}As$ layer. Results from this and other areas of similar material assessment will be described in a subsequent publication.

Note

During the period while this paper was under review, a publication on the same topic (42) has appeared in the literature. We have carried out anodic etching experiments on n^+-GaAs exactly as described by

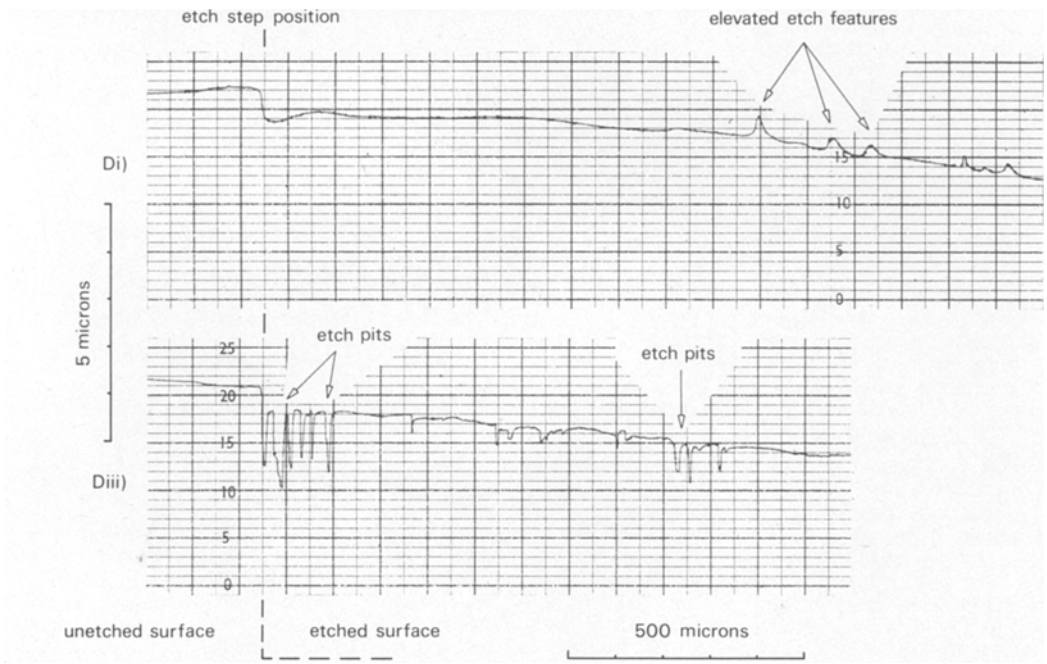

Fig. 9. "Talysurf" profiles of the etched surfaces photographed as Di and Diii in Fig. 8.

Greene in an attempt to classify the defect revealing conditions according to our Fig. 8. The most important distinction is that no deliberate illumination is included in Greene's experimentation. Thus, automatically, the rather "heavy-weight" conditions imposed (maximum current density 2 mA cm^{-2} and cell voltage 10V) lead to a defect resolution of types ii and iii in Fig. 8, depending somewhat on the level of ambient illumination. These are not the most sensitive conditions. For example, only the prephotosaturation current density etching of sample S in Fig. 8 (Si) resolves the high density of nodular features which we suspect are related to impurity precipitation defects in Si-doped n^+-GaAs.

Acknowledgments

We are grateful to Mrs. M. A. G. Halliwell for pursuing the x-ray topographic study referred to in this paper, and for many useful discussions concerning this aspect of the work. Further experimental design and assistance was given by R. M. Redstall, M. C. Case, and J. C. Regnault. We are also indebted to Dr. T. Ambridge and Dr. R. Heckingbottom for their interest and advice.

This paper is published by permission of the Director of Research of the British Post Office.

Manuscript submitted March 21, 1977; revised manuscript received Oct. 31, 1977.

Any discussion of this paper will appear in a Discussion Section to be published in the December 1978 JOURNAL. All discussions for the December 1978 Discussion Section should be submitted by Aug. 1, 1978.

Publication costs of this article were assisted by the Post Office Research Centre.

APPENDIX

Use has been made in these studies of the anodic capacitance and polarization characteristics of n-GaAs.

Electrode capacitance.—The only systematic examination of the depletion characteristics of GaAs/electrolyte contacts is that due to Benard and Handler (29), who determined specifically the semiconductor surface potentials but used only strongly acidic media. The collection of data assembled in Fig. 1 includes that measured for the electrolytes used here, and confirms that the n-type semiconductor surface is in substantial depletion under open-circuit conditions. One noteworthy aspect is that the band-bending ($|\psi_s^n|$) for the electrolytic contact appears to exceed almost everywhere in the pH range the values measured for n-GaAs/metal junctions ($-0.80V \geqq \psi_s^n \geqq -0.95V$) by Mead (30). There is also present a systematic variation of ψ_s^n with pH, and this produces a differential resolution of the crystallographic defects in step 2 etching conditions, just as that obtained by variation of the bias voltage and pictured in Fig. 8. The highest etch discrimination is procured therefore with acidic media, where the field strength in the depletion layer is lower. Note that Fig. 1 will not apply to electrolytes containing strong oxidizing agents (31).

Electrode dissolution and passivation.—It is well known that the anodic dissolution of the wide bandgap semiconductors requires the participation of holes. Pleskov (32) first confirmed that this was the case for GaAs, having investigated the anodic currents gained using both acidic and alkaline electrolytes. The curve shown as Fig. 2i here, where use has been made of the complexant electrolyte Tiron, is of the same classical form (33, 34) and yields, over-all, two important advantages in the topographical etching studies. First, the anodic reaction has a strict six-electron equivalence (35), which allows the integrated current density to be converted automatically to the average dissolution depth. Second, it allows the electroetching to occur without interference from insoluble products at the electrode surface, in contrast to, say, sulfuric acid solutions which leave precipitated arsenious oxide (26). Importantly also, the electrolyte is acidic (see a, above).

Conversely, the anodic polarization curve obtained using the phosphate electrolyte (Fig. 2ii) shows passivation characteristics similar to those observed for various GaAs electrodes by Harvey (36, 37). Since curves 2i and 2ii were recorded under identical illumination conditions, it is clear that the straightforward photosaturation limitation present in the first instance has been replaced in 2ii by a kinetic restraint due to product insolubility.

From Fig. 3 it is apparent that a mixture of the two electrolytes allows both of these individual characteristics to appear in succession. Specifically, the addition of the complexant (Tiron) to the barrier oxide forming electrolyte (NaH_2PO_4) has led to a large increase in the steady-state current density achievable in the presence of a uniform anodic oxide film (compare point B in Fig. 3 with the original passivation curve 2ii). As yet we have been unable to clearly resolve the individual roles of photoinjection and Schottky barrier breakdown in the supply of holes for the over-all dissolution reaction. A six-electron equivalence is maintained however, with a 1 mA cm^{-2} current density corresponding to a continuous removal rate of 1.7 μm per hour. Some experimental observations concerned with the effect of aqueous electrolyte composition on the outcome of GaAs anodization have been published by Schwartz *et al.* (38). In comparison, the specific complexant action of Tiron, as set out above for the mixed electrolyte, is rather better defined than the anion-type dependencies noted by Schwartz *et al.* Also, the use of an electrochemical regime where oxide dissolution is uniformly enhanced for the machining of GaAs (see step 1 in Fig. 5) was not dealt with. In fact, one particularly important application (the precise thickness trimming of epitaxial layers) has generally been subjected to a noncontinuous method, where, in separate steps, the oxide is first grown and then removed under open-circuit dissolution conditions (3, 39, 40). Clearly this multiple-stage processing may lead to some cumulative inaccuracy in assessing the over-all material removal.

REFERENCES

1. T. Ambridge, C. R. Elliott, and M. M. Faktor, *J. Appl. Electrochem.*, **3**, 1 (1973).
2. T. Ambridge and M. M. Faktor, *ibid.*, **5**, 319 (1975).
3. W. C. Niehaus and B. Schwartz, *Solid-State Electron.*, **19**, 175 (1976).
4. H. Hasegawa and H. L. Hartnagel, *This Journal*, **123**, 713 (1976).
5. G. R. Woolhouse, A. E. Blakeslee, and K. K. Shih, *J. Appl. Phys.*, **47**, 4349 (1976).
6. J. I. Pankove, "Optical Processes in Semiconductors," Prentice-Hall, Inc., Englewood Cliffs, N.J. (1971)
7. D. J. Stirland and B. W. Straughan, *Thin Solid Films*, **31**, 139 (1976).
8. S. Komiya, K. Akita, Y. Nishitani, S. Isozumi, and T. Kotani, *J. Appl. Phys.*, **47**, 3367 (1976).
9. H. Kressel, in "Fundamentals of Fibre Optic Communication," M. K. Barnoski, Editor, p. 109, Academic Press, New York (1976).
10. M. S. Abrahams and C. J. Buiocchi, *J. Appl. Phys.*, **36**, 2855 (1965).
11. F. Kuhn-Kuhnenfeld, *This Journal*, **119**, 1063 (1972).
12. T. Saitoh, S. Matsubara, and S. Minagawa, *This Journal*, **122**, 670 (1975).
13. E. G. Bremner, T. Ambridge, and C. R. Elliott, *J. Phys. E*, **6**, 326 (1973).
14. T. Ambridge and M. M. Faktor, *J. Appl. Electrochem.*, **4**, 135 (1974).
15. G. Beilby, "Aggregation and Flow of Solids," Macmillan Publishing Co., Inc., London (1921).
16. R. T. Holm, J. W. Gibson, and E. D. Palik, *J. Appl. Phys.*, **48**, 212 (1977).
17. M. A. G. Halliwell, J. B. Childs, and S. O'Hara, *Inst. Phys. Conf. Ser.*, **17**, 98 (1973).
18. G. A. Rozgonyi and D. C. Miller, *Thin Solid Films*, **31**, 185 (1976).
19. D. Laister and G. M. Jenkins, *J. Mater. Sci.*, **8**, 1218 (1973).
20. K. K. Shih, G. R. Woolhouse, A. E. Blakeslee, and J. M. Blum, *Inst. Phys. Conf. Ser.*, **24**, 165 (1975).
21. G. B. Stringfellow and P. E. Greene, *J. Appl. Phys.*, **40**, 502 (1969).
22. A. G. Milnes, "Deep Impurities in Semiconductors," p. 103, Wiley-Interscience, New York (1973).
23. A. R. Peaker, B. Hamilton, D. R. Wight, I. D. Blenkinsop, W. Harding, and R. Gibb, *Inst. Phys. Conf. Ser.*, **33a**, 326 (1977).
24. C. LeMay, *J. Appl. Phys.*, **34**, 439 (1963).

25. D. J. Stirland, *Inst. Phys. Conf. Ser.*, **33a**, 150 (1977).
26. J. P. Krumme and M. E. Straumanis, *Trans. Met. Soc. AIME*, **239**, 395 (1967).
27. M. M. Faktor, D. G. Fiddyment, and M. R. Taylor, *This Journal*, **122**, 1566 (1975).
28. T. J. Hayes, A. Rasul, and S. M. Davidson, *J. Electron. Mater.*, **5**, 100 (1976).
29. D. J. Benard and P. Handler, *Surf. Sci.*, **40**, 141 (1973).
30. C. A. Mead, *Solid-State Electron.*, **2**, 1023 (1966).
31. H. Gerischer, *Surf. Sci.*, **18**, 97 (1969).
32. Yu. V. Pleskov, *Doklady Akad. Nauk SSSR*, **143**, 1399 (1962).
33. W. H. Brattain and C. G. B. Garrett, *Bell Syst. Tech. J.*, **34**, 129 (1955).
34. W. W. Gartner, *Phys. Rev.*, **116**, 84 (1959).
35. H. Gerischer, *Ber. Bunsenges.*, **69**, 578 (1965).
36. W. W. Harvey, *This Journal*, **114**, 472 (1967).
37. W. W. Harvey and J. Kruger, *Electrochim. Acta*, **16**, 2017 (1971).
38. B. Schwartz, F. Ermanis, and M. H. Brastad, *This Journal*, **123**, 1089 (1976).
39. D. L. Rode, B. Schwartz, and G. D. Weigle, *Solid-State Electron.*, **17**, 1119 (1974).
40. H. Muller, F. H. Eisen, and J. W. Mayer, *This Journal*, **122**, 651 (1975).
41. W. H. LaFlere, F. Cardon, and W. P. Gomes, *Surf. Sci.*, **44**, 541 (1974).
42. L. I. Greene, *J. Appl. Phys.*, **48**, 3739 (1977).

On the Nature of Fixed Oxide Charge

S. I. Raider*,[1] and A. Berman

IBM System Products Division, East Fishkill Facility, Hopewell Junction, New York 12533

ABSTRACT

An oxidation-induced fixed oxide charge Q_{ss} is known to be generated in the SiO_2-Si interfacial region. In the light of recent determinations of the composition and width of this interfacial transition region, a reexamination of the nature of this charge is undertaken. A model, consistent with known transition region composition, is proposed in which a positively charged silicon-oxygen complex is formed as an intermediate reaction product of the oxidation process. This intermediate may be trapped within the transition region when the oxidation reaction is terminated by quenching in the oxidizing ambient. The concentration of this complex is proportional both to the excess oxygen concentration and to the nonoxidized Si-Si bond density in the transition region. The model is also consistent with the dependence of Q_{ss} on such factors as oxidant pressure, oxidation temperature, inert-gas annealing, and substrate orientation.

Electrically active sites such as fixed oxide charge, Q_{ss} form in the oxide film at or near the SiO_2-Si interface (1) during the oxidation reaction. Their formation occurs within the same region in which Si is incompletely oxidized and within which the oxidation process takes place (2, 3). The number of nonoxidized Si atoms present within this transition region cannot be identified with Q_{ss}. The density of these charge sites after oxidation (10^{12} cm^{-2}) (1, 4) is significantly lower than the nonoxidized Si-Si bond density (10^{15} cm^{-2}) within the transition region. Q_{ss} is reduced further (to 10^{10}-10^{11} cm^{-2}) by postoxidation annealing treatments (1, 4). The magnitude of Q_{ss} depends intimately upon the thermal oxidation process (1). Despite numerous studies, the relationship between thermal oxidation and Q_{ss}, as well as the chemical nature of Q_{ss} is not well understood. Control of fixed oxide charge densities, which are of technological importance, remains largely empirical.

Recently, the composition and width of the SiO_2-Si interface, formed by thermal oxidation of <100> and <111> oriented Si surfaces were characterized by analysis of x-ray photoelectron spectroscopy (XPS) data (5-8). Changes in Si chemical bonding at this interfacial region were derived from XPS spectra (5, 8). Although the detection limit of x-ray photoelectron spectroscopy is approximately 10^{13} cm^{-2} and does not provide a means for direct observation of the sites responsible for Q_{ss}, the XPS findings do provide a new picture of the transition region within which these electrical instabilities must be understood. We have therefore reconsidered the thermal oxidation process and the related chemistry that occurs at an SiO_2-Si transition region and that may influence the oxide charge densities.

Fixed Oxide Charge

The properties of fixed oxide charge have been summarized in several papers (1, 4) and review articles (9-12) and are only briefly described here. These charges form a positive space charge in the oxide film during the thermal oxidation process and induce a negative image charge in the Si substrate. Fixed oxide charges are stable under moderate temperature-bias conditions and are unaffected by changes in surface potential. Densities are dependent upon substrate orientation with Q_{ss}<111> > Q_{ss}<100>. Chemical etching (1) and internal photoemission experiments (13, 14), as well as the dependence of Q_{ss} upon substrate orientation, indicate that Q_{ss} is near to the substrate. For example, results of internal photoemission experiments suggest that most of the charge is located at less than 20Å from the substrate and is spatially distributed within the SiO_2-Si transition region.

Factors that influence Q_{ss} include oxidation and annealing ambients and the oxidation temperature. Charge densities reflect the final oxidation or annealing conditions. The formation or reduction of Q_{ss} is reversible provided that steady-state conditions are achieved. In a reactive dry oxygen ambient, Q_{ss} increases with decrease in oxidation temperature. An example taken from the earlier literature (1) shows that Q_{ss} is about 4.2×10^{11} cm^{-2} after 2000Å thick films have been annealed to minimize Q_{ss} and subsequently oxidized at 550°C. After oxidation of Si at 1200°C, Q_{ss} is 2×10^{10} cm^{-2}. Varying the rate at which a sample is pulled from a hot zone in an oxidation furnace is equivalent to adjusting the final effective oxidation temperature at which the oxidation reaction is quenched, thereby altering Q_{ss}. High temperature an-

* Electrochemical Society Active Member.
[1] Present address: Thomas J. Watson Research Center, Yorktown Heights, New York 10598.
Key words: silicon, oxidation, SiO_2-Si interface, electrical instabilities, surface states.